SEPERATION OF COSEISMIC AND POSTSEISMIC SIGNALS OF SUMATRA ANDAMAN EARTHQUAKE AND INDIAN OCEAN EARTHQUAKE

NOVEMBER 2019

VUMMMIDI NARAYANEE

4898699

Assessment Committee:

Dr. R.E.M (Riccardo) Riva, TU Delft (Chairman)

Dr.ir. D.B.T. Broerse, TU Delft (Daily Supervisor)

Dr.ir. W. (Wouter) van der Wal (External Supervisor)

Table of Contents:

1. Introduction:

Earthquakes are one of the major geophysical processes that can cause large changes in the internal mass redistribution. The normal geodetic methods like GPS, InSAR and tsunami sensors measure or map only the changes that are happening on the surface. To map the density changes or the redistribution happening below the earth, Satellite gravimetry is one of the best methods to be used. Though Satellite gravimetry has less spatial resolution, it can map the changes caused internally (below the earth surface) due to the large earthquakes. The ocean floor movement, crustal dilatation and density changes caused by both the land and underwater earthquakes can be mapped. Therefore, the changes in the Gravity field before, during and after the occurrence of earthquake play a major role in determining the internal mass changes that has occurred due to the earthquake.

In the recent past, Sumatra-Andaman earthquake was one of the large magnitude earthquakes with a magnitude of Mw 9.1. This earthquake occurred on 26th December 2004. Following this earthquake, many other smaller earthquakes have occurred in this region in the following years. The other major earthquake that I have taken into account is the off coast Northern Sumatra earthquake (also called as Indian Ocean earthquake) which occurred on 11th April 2012 with a magnitude of Mw 8.6. The above mentioned 2004 earthquake occurred near the plate boundary between the Indian plate and Sunda plate. On other hand, the above mentioned 2012 earthquake occurred within the Indian plate.

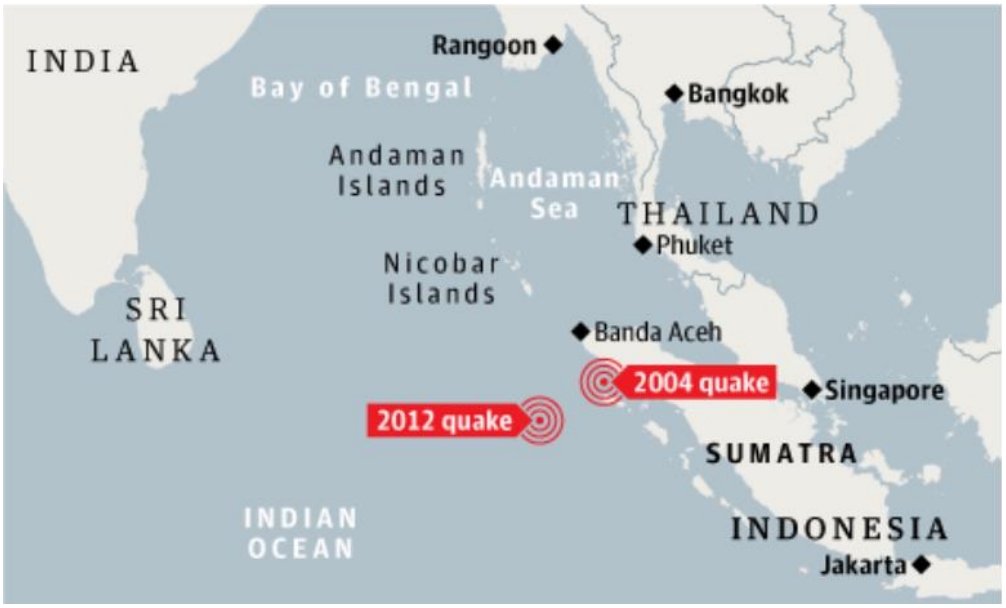

Figure 1: Represents the location of the two earthquakes (Sumatra Andaman earthquake and Indian Ocean earthquake). Source: Golluoglu, E. (2012). Indonesia lifts tsunami alert after 8.6-magnitude earthquake. Retrieved from https://www.theguardian.com/world/2012/apr/11/indonesia-tsunami-warning-earthquake-aceh

The gravity field changes associated with the earthquake are analysed using the GRACE (Gravity Recovery and Climate Experiment) data. GRACE can track the temporal variations in the gravity field and therefore information on mass redistribution can be achieved. There have been many studies already carried out using the GRACE data to analyse the coseismic and postseismic effects

of the earthquakes. The previous studies mainly concentrated on the separation of earthquake signals from various other signals and noises to understand the internal mass redistribution. In addition to this, previous studies have made validation of using GRACE data for the earthquake analysis using the geodetic methods.

In this paper as mentioned above, I have considered two earthquakes (Sumatra-Andaman earthquake, 2004 & Indian Ocean earthquake, 2012). I have taken a new initiative to separate the long term postseismic trend (2004 earthquake) from the coseismic term of 2004 earthquake and I have removed the effects of the 2012 earthquake (both coseismic and postseismic term) as well. I have carried out this decoupling process using the GRACE monthly solutions of spherical harmonics. This process is done by calculating the gravity disturbances from GRACE monthly solutions to understand the internal mass redistribution.

1.1. Description on region of earthquakes:

Sumatra earthquake occurred to the west of the Northern Sumatra region. It occurred due to the thrust faulting at the plate boundary between the Indian plate and the Burma microplate. There was a built-up stress in this region due to the subduction of the Indian plate under the Burma microplate. This built-up stress was released during the Sumatra earthquake. In a wider sense, the Indian and the Australian plates are moving north-east in a direction towards the Eurasian plate. Therefore, there is an oblique convergence caused near the Sunda trench.

Indian Ocean earthquake is one of the largest strike-slip earthquakes because this high magnitude earthquake has occurred in the interior of the Indian plate and not at the boundaries (100-300 Km west of the Sunda megathrust). Additionally, this strike-slip faulting occurred differently (first three faults were perpendicular to each other and then there was a jump parallel to the third fault causing the forth fault). There was a large magnitude after-shock after this main event creating a history of large inter-plate earthquake. (Oskin, 2019)

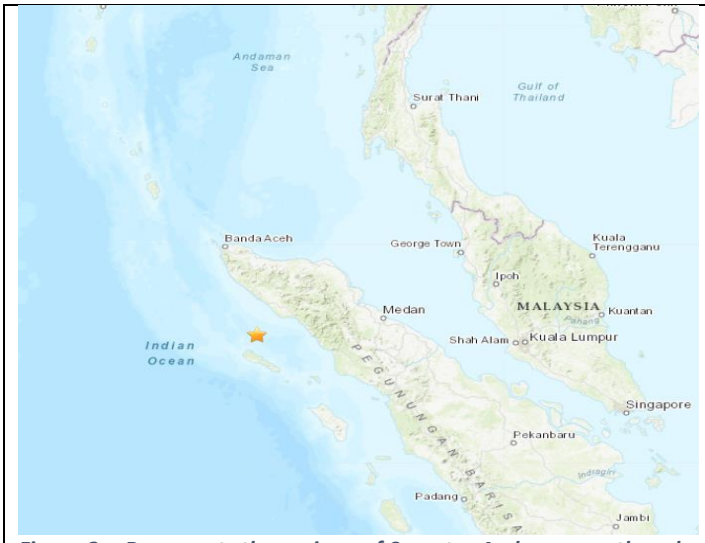

Figure 2a: Represents the regionn of Sumatra Andaman earthquake with the epicentre marked with the orange star (Source: USGS)

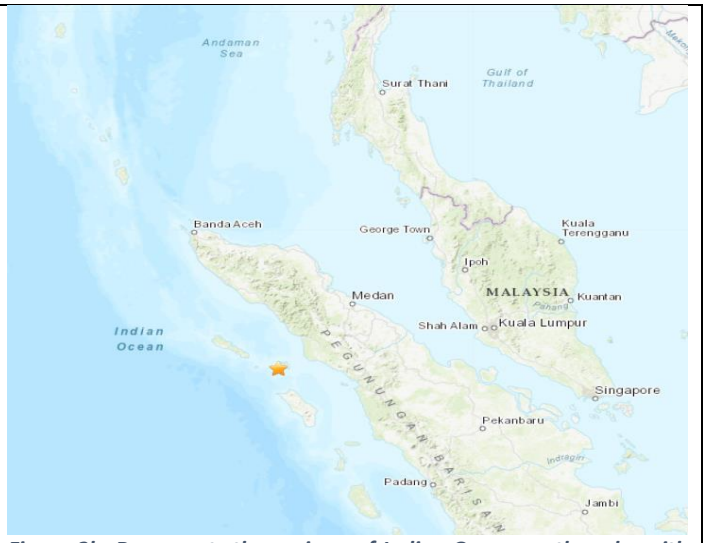

Figure 2b: Represents the regionn of Indian Ocean earthquake with the epicentre marked with the orange star(Source: USGS)

2. Previous studies:

In this part, I have reviewed some of the previous studies to know more about the usage of GRACE data to analyse the earthquake and its coseismic and postseismic gravity patterns. Han (2006) was one of the foremost to deal with the gravity changes induced by the Sumatra-Andaman earthquake. This paper gives a detailed information on the data used and how the data is processed for further analysis. In addition to this, information is given on filtering the gravity signals and the method to reduce the signal from the surrounding areas. Finally, the gravity patterns obtained from GRACE data was compared to the fault slip data which was used to model the uplift and subsidence. Following this, Ogawa & Heki (2007) have given more insight on the role of water in postseismic relaxation of Sumatra Andaman earthquake. This study suggests that the relaxation of the geoid depression was mainly due to the water diffusion. In addition to this, the polarity reversal between coseismic and post seismic geoid changes and the role of water in regards to poro-elastic rebound was discussed. Finally, a new face was added to satellite gravimetry as it was able to reveal the postseismic healing of geoid by diffusive adjustment. Adding to this, de Linage et al. (2009) discuss on the separation of coseismic and post seismic signals of the Sumatra earthquake using GRACE data (in terms of geoid height and gravity anomalies). On the other hand, this study carries out a complete modelling using normal mode summation to find the coseismic gravity changes. The gravity patterns obtained by fitting an equation to the GRACE data was compared to the results obtained through modelling. As an add-on, the gravitational effect of the Ocean mass redistribution after the earthquake was discussed which was not addressed in the previous studies.

As an extension to the previous study, Broerse, Vermeersen, Riva & van der Wal (2011) discuss about the deformation of ocean floor, corresponding sea level equation and in turn gravity changes due to the change in sea level. The computations was carried out using the sea level equation and the normal mode model. This study interprets the importance of the sea level change and its effect on the gravity patterns produced due to the geoid height changes. The reason for the reduction in the positive coseismic geoid anomaly was discussed and the role of sea-level in this effect. Therefore, this study concludes the necessity to include the ocean mass re-distribution while modelling the gravity changes with respect to the sub-oceanic earthquakes. All the previous studies had taken steps to study the gravity patterns and respective changes on the earth, but Han, Riva, Sauber & Okal (2013) discuss on quantifying the gravity changes for the great earthquakes that have occurred in the recent past. The quantification was done for the past 10 years of GRACE gravity field data. The source parameters of the moment tensor and double-couple were estimated using the gravity data spherical harmonic normal-mode formulation. Sumatra Andaman earthquake (2004), Maule earthquake (2010), Tohoku-Oki earthquake (2011), Indian Ocean earthquake (2012) and Bengkulu earthquake (2007) were the earthquakes considered for the processing. The processing was done by spatial localization of the gravity signals, thereby the local signals can be separated from the global signals. The formulated Inverse models were used to find the fault parameters using the GRACE gravity data for each of the above mentioned earthquakes, thereby this provided a new domain for the usage of GRACE gravity data to constrain the fault parameters.

As we know, the gravity changes can map the internal density changes and internal mass redistribution. There was no previous studies discussing much on the density changes and their

relationship to the results obtained from GRACE gravity data. But Broerse, Riva, Simons, Govers & Vermeersen (2015) have dealt with the rheology contrast that has occurred in the Sumatra earthquake region using GRACE and GPS. The contrast was identified using the different relaxation time obtained during the investigation of both the data (GRACE and GPS). To substantiate this, 1-D viscoelastic models were used. Finally, this study concludes about the GRACE sensitivity to map the relaxation happening in the asthenosphere below the ocean. On other hand, GPS sensitiveness to map the relaxation in continental asthenosphere.

All the studies discussed above, dealt with the Sumatra–Andaman earthquake, except Han, Riva, Sauber & Okal (2013) which deals with both the Sumatra-Andaman earthquake and the Indian Ocean earthquake. But Han, Sauber & Pollitz (2015) discuss about the gravity changes due to the strike-strip faulting of the Indian Ocean earthquake. This earthquake occurred in the same region as the Sumatra earthquake, therefore special care was taken to remove the postseismic signal of 2004 earthquake and the climate signals. The coseismic and postseismic gravity patterns with compression and dilatational quadrant was well explained. In addition to this, the vertical motion of the land was mapped using the GPS data and was compared to the GRACE data processing. Therefore, GPS data was used to validate the GRACE data processing.

3. Methodology:

The GRACE data that I have used for processing was taken from ITSG-Grace 2018. In order to ensure that, I have used a reliable time series of GRACE data for my processing. Kvas.et.al (2019) was reviewed, which finally ensured that the ITSG-Grace time series were consistent with the official GRACE time series like CSR, GFZ.etc. Therefore, I used the ITSG-monthly solutions (spherical harmonic coefficients) of degree and order up to 60 from January 2003 to December 2016 for analysis. The higher degrees were eliminated to reduce the high frequency noise in the data. The months for which the GRACE data was available was taken for analysis excluding the months in which the earthquake occurred. The signal to noise ratio of the gravity signals was enhanced by using the monthly solutions for a longer time period.

3.1 Procedure description:

To start with, I removed the long term mean from both the positive and negative stokes coefficients. These coefficients were converted into $\Delta\bar{C}_{lm}$ and $\Delta\bar{S}_{lm}$. These coefficients of spherical harmonics were converted into coefficients of gravity disturbances using the following formula:

$$\bar{C}_{lm}^{(\delta g)} = \frac{GM}{R^2} \triangle \bar{C}_{lm}(l+1) \tag{1}$$

I considered gravity disturbances instead of the gravity anomalies or geoid height as it mainly maps to the internal mass redistribution and the density changes that are happening due to the earthquake. In addition to this, I used Gaussian filtering to remove the short wavelength noise. Therefore the coefficients of gravity disturbances calculated using equation (1) was multiplied

with the Gaussian filter coefficients $\left(C_l^{(W)}\right)$ as shown in equation (2). The Gaussian filter coefficients were calculated using the following recursive scheme as shown in equation (3)

$$\bar{C}_{lm}^{\delta g_w} = \frac{4*pi}{(2*l)+1} * \bar{C}_{lm}^{\delta g} \quad * \quad C_l^{(W)} \tag{2}$$

$$C_l^{(W)} = \frac{2l+1}{2} W_l$$

$$\begin{cases} W_0 = \dfrac{1}{2\pi} \\ W_1 = \dfrac{1}{2\pi}\left(\dfrac{1+e^{-2b}}{1-e^{-2b}} - \dfrac{1}{b}\right) \\ W_{l+1} = -\dfrac{2l+1}{b} W_l + W_{l-1} \end{cases}$$

$$b = \frac{ln(2)}{1-\cos\psi_0} \tag{3}$$

φ_o is the filter half width. I have considered the filter half-width as 300 Km (Initially, the filter half width value was taken as 350 Km from (Ogawa & Heki, 2007) and (de Linage et al., 2009). Then the value was finalized by the trial and error method to get clear gravity patterns).

Once the short wavelength noise was removed, the filtered coefficients were fit to be used for the calculation of gravity disturbances. Initially, I chose my region of interest in such way that I am able to cover both the earthquakes in one region with some additional space around it. Theta (θ) and lambda (λ) which are given as the input for equation (4) were considered in accordance to the chosen region of interest. In my case, I chose my latitude ranging from 15°N - 10°S and then it was converted to co-latitude for further usage as theta in equation (4). Additionally, I chose my longitude ranging from 85°E to 110°E which was considered as lambda for further usage in equation(4). With the above mentioned range of theta and lambda, the grid size resulted in 26*26 grid (each grid = 1° * 1°). Finally, I used equation (4) to convert the coefficients of gravity disturbances into gravity disturbances values for every grid point.

$$\delta g = \sum_{l,m} \bar{C}_{lm}^{\delta g_w} * \bar{Y}_{lm}(\theta, \lambda) \tag{4}$$

$\bar{Y}_{lm}(\theta, \lambda)$ in equation (4) represents 4-π normalised surface spherical harmonics. This is calculated using the following formula in equation (5):

$$\bar{Y}_{lm}(\theta,\lambda) = \bar{P}_{l,|m|}(cos\theta) \begin{cases} cos(m\lambda) & m \geq 0 \\ cos(|m|\lambda) & m < 0 \end{cases} \tag{5}$$

Where $\bar{P}_{l,|m|}$ is the Normalized Associated Legendre function and it is formulated using the following formulas and recursive scheme:

1. "Diagonal" recursion:

$$\bar{P}_{0,0}(t) = 1,$$
$$\bar{P}_{1,1}(t) = u\sqrt{3} \qquad \text{with} \quad u = \sqrt{1-t^2},$$
$$\bar{P}_{l,l}(t) = u\sqrt{\tfrac{2l+1}{2l}}\,\bar{P}_{l-1,l-1}(t) \qquad (l \geq 2).$$

2. Recursion per degree:

$$\bar{P}_{l,m}(t) = \begin{cases} a_{l,m}\,\dfrac{t}{u}\,\bar{P}_{l,m+1}(t) & (m = l-1) \\ a_{l,m}\,\dfrac{t}{u}\,\bar{P}_{l,m+1}(t) - b_{l,m}\bar{P}_{l,m+2}(t) & (0 \leq m \leq l-2) \end{cases}$$

$$\text{where} \qquad a_{l,m} = \frac{2}{\sqrt{1+\delta_{0,m}}}\,\frac{m+1}{\sqrt{(l-m)(l+m+1)}}$$

$$\text{and} \qquad b_{l,m} = \frac{1}{\sqrt{1+\delta_{0,m}}}\,\frac{\sqrt{(l+m+2)(l-m-1)}}{\sqrt{(l-m)(l+m+1)}}.$$

(Note - All the equations in this section 3.2 up to this point are the formulas taken from the notes provided by Professor Pavel Ditmar during the course of Gravity, Geodynamics and Climate change (CIE4610)).

On implementing the above steps, I did obtain a grid (in accordance to the length of theta and lambda) with gravity disturbances calculated for each of the grid. These gravity disturbances calculated for the grid can be used for estimating the coseismic and postseismic gravity changes of the earthquake. With the gravity changes obtained for the particular region, one would obtain a picture of the internal mass redistribution that is associated with the earthquake.

To obtain the coseismic and postseismic gravity changes, the seasonal climate signals and tidal-aliasing signals have to be removed. Therefore, the following fitting equation (6) was used to obtain the required gravity change signals and to remove the other signals. The equation (6) was taken from Broerse, Riva, Simons, Govers & Vermeersen (2015) and then it was modified in-accordance to the current scenario with two earthquakes. As the above mentioned paper addresses one earthquake, the equation was modified in-accordance to address two earthquakes (Sumatra-Andaman earthquake, 2004 and Indian Ocean earthquake, 2012) and find individual coseismic and postseismic gravity changes.

$$y = \mathrm{a} * \cos(2 * pi * t) + \mathrm{b} * \sin(2 * pi * t) + \mathrm{c} * \cos(2 * pi * \omega * t) + \mathrm{d} * \sin(2 * pi * \omega * t) + e * \cos(4 * pi * w * t) + f * \sin(4 * pi * w * t) + g + H(t - t_{eq})\left(h + i * ln * \left(1 + \frac{t - t_{eq1}}{\tau_1}\right)\right) + H(t - t_{eq})\left(j + k * ln * \left(1 + \frac{t - t_{eq2}}{\tau_2}\right)\right) \quad (6)$$

- coefficients a-f represent the annual and semi-annual constants (climate signals)
- coefficient g represents the bias
- H represents the Heaviside function
- co-efficient h represents the coseismic discontinuity for 2004 earthquake
- $i * ln * \left(1 + \frac{t - t_{eq1}}{\tau_1}\right)$, represents the complete postseismic term for 2004 earthquake. Co-efficient i represents the scaling factor.
- t_{eq1} represents the epoch of first earthquake and co-efficient τ_1 represents the relaxation time associated with 2004 earthquake
- co-efficient j represents the coseismic discontinuity for 2012 earthquake
- $k * ln * \left(1 + \frac{t - t_{eq2}}{\tau_2}\right)$, represents the complete postseismic term for 2012 earthquake. Co-efficient k represents the scaling factor.
- t_{eq2} represents time of second earthquake and co-efficient τ_2 represents the relaxation time associated with 2012 earthquake
- Finally, t is the time in years.

To calculate the coseismic and postseismic gravity changes associated with two earthquakes, I performed non-linear least squares using the above fitting function (equation (6)) to the gravity disturbances calculated for the complete grid and for the complete time series of gravity disturbances. The fitting function contains 13 coefficients (a-k, which has to be estimated for the complete grid and the whole time series), so I assigned 13 initial values, 13 upper and lower constraints to perform the inversion. The inversion was done for the whole grid at once using the 'lsqcurvfit' function in MATLAB using the default algorithm ('Trust-region reflective').

The following table represents the assigned initial values, upper and lower constraints for the coefficients:

Coefficients	Initial Value (micro gals)	Lower limit (constraint) - (micro gals)	Upper limit (constraint) - (micro gals)
a-g	5	-20	20
h	5	-30	30
i	3	0	10
j	5	-30	30
k	3	0	20

(Note – The above Initial values was obtained in a trial and error method. Initially, I did the inversion without the constraints (similar initial values) and checked the value ranges for each of the coefficients. Depending on the value range and few trial and errors, the upper and lower constraints were defined which is mentioned in the above table.)

Once the estimates of the above mentioned coefficients were calculated, I used 'nlparci' function to calculate the 95% confident interval for the estimates calculated using the non-linear least square inversion. This resulted in values for upper and lower bounds (confidence interval) for each of the estimated values. Finally, I calculated the root mean square of the residuals (obtained from the difference between the calculated and the estimated gravity disturbances) to show the error distribution in the region of interest.

4. Results and Explanation:

The estimated values for each of the co-efficient (from the 13 coefficients) is a matrix, with a size similar to that of the grid (26*26). Therefore the estimated values of h, the complete post seismic term of 2004 earthquake ($i * ln * \left(1 + \frac{t-t_{eq1}}{\tau_1}\right)$)-(equation for the complete postseismic term) are displayed as spatial plots to identify the change in gravity patterns during and after the 2004 Sumatra-Andaman earthquake. The following figure 4a represents the coseismic gravity pattern obtained for the Sumatra earthquake. Dipole gravity pattern is obtained. Gravity decrease (around 15 $\mu gals$) is seen in the region of Northern Sumatra and Andaman Sea. While, the gravity increase (around 6-7 $\mu gals$) is long and elongated. It is present to the west of the Northern Sumatra region extending from 0° to 15°N. Figure 4b represents the uncertainty of the gravity signals obtained for the coseismic term of Sumatra earthquake. It can be seen that, the uncertainty is higher near the north-western part of the Northern Sumatra region. The uncertainty ranges from 0.865 – 0.875 $\mu gals$. (In my case, uncertainty is referred as the difference obtained between the upper limit (95% confidence interval) of the estimated value and the estimated value. This value is equal to the value obtained by the difference between the lower limit of the estimated value and the estimated value. Therefore, anyone can be considered. In my case, I have considered the upper limit and the difference is taken which is finally plotted spatially to know the region of high and low uncertainties. This definition of uncertainty remains the same for all the other estimated terms as well).

Following this, figure 5a represents the gravity pattern of complete postseismic term of the Sumatra earthquake ($i * ln * \left(1 + \frac{t-t_{eq1}}{\tau_1}\right)$)-(equation for the complete postseismic term). To represent this complete postseismic term of Sumatra earthquake as a spatial plot as shown in the figure 5a, t value was taken as 14 (Last epoch considered in the time series. The time series starts with 0 representing the year 2002 and 14 representing the year 2016). In addition to this, t_{eq1} was taken as the epoch in which the Sumatra earthquake happened (in terms of years with the actual day represented in decimal following the number that represents the year 2004 in accordance to the considered time series.), estimated i and τ_1 (3.169 – estimated value for the relaxation time of

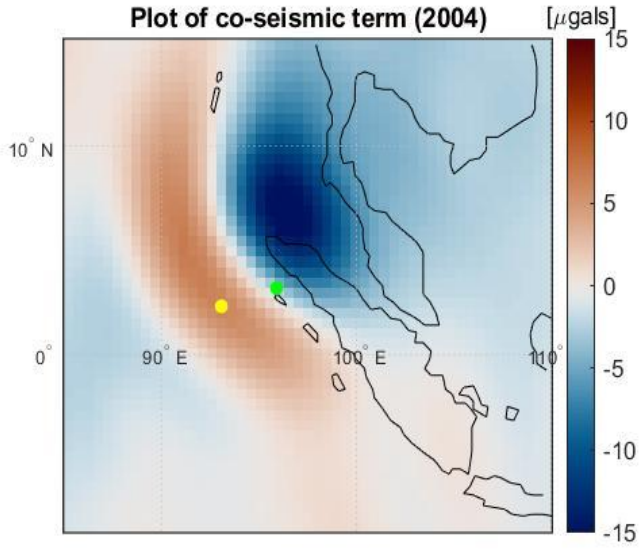

Figure 4a: Represents the coseismic gravity pattern for the Sumatra earthquake.(Green dot represents the epicentre of the Sumatra earthquake and yellow dot represents the epicentre of the Indian Ocean earthquake)

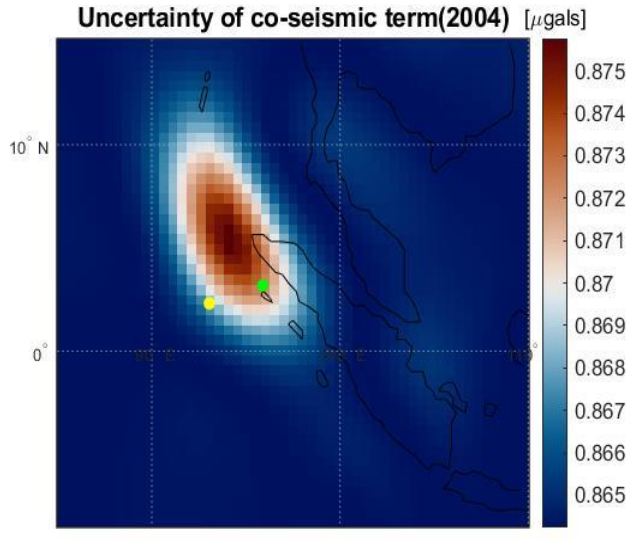

Figure 4b: Represents the uncertainty of the gravity signals for the coseismic gravity pattern of the Sumatra Andaman earthquake. (Green dot represents the epicentre of the Sumatra earthquake and yellow dot represents the epicentre of the Indian Ocean earthquake)

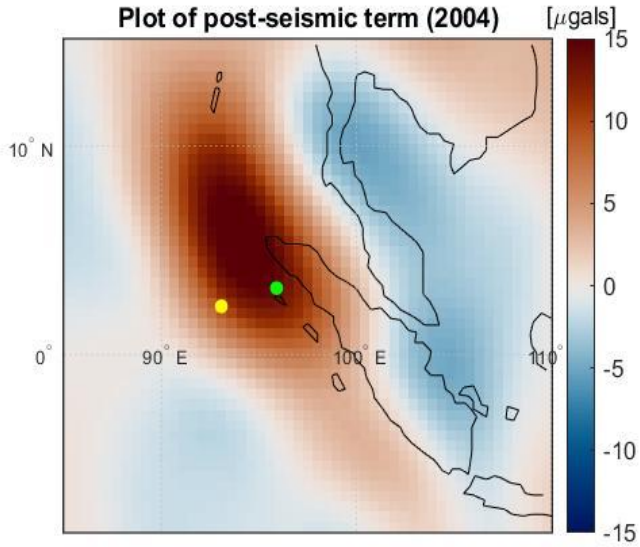

Figure 5a: Represents the postseismic gravity pattern for the Sumatra earthquake. (Green dot represents the epicentre of the Sumatra earthquake and yellow dot represents the epicentre of the Indian Ocean earthquake)

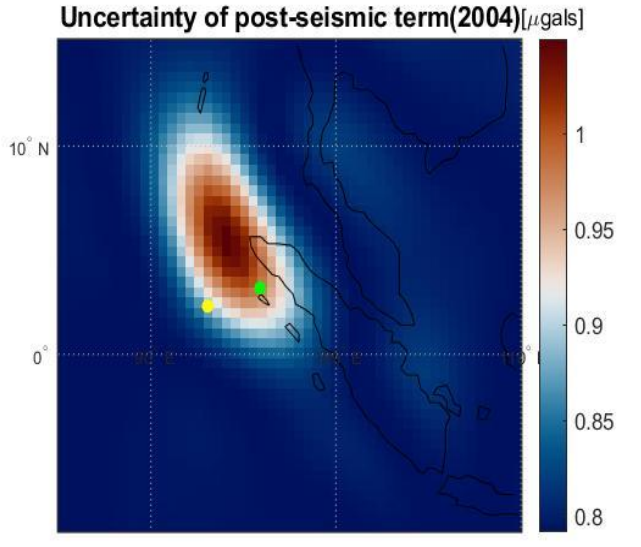

Figure 5b: Represents the uncertainty of the gravity signals for the postseismic gravity pattern of the Sumatra earthquake.(Green dot represents the epicentre of the Sumatra earthquake and yellow dot represents the epicentre of the Indian Ocean earthquake)

2004 earthquake) values were also taken and substituted in the equation shown for the complete postseismic term.

As previously said, figure 5a represents the gravity patterns obtained after the earthquake (spatial representation of postseismic gravity signals). Tri-polar pattern can be seen with the gravity increase at the centre (around $15\mu gals$). It is surrounded by the gravity decrease on both the sides

(around 4 $\mu gals$ to 5 $\mu gals$). Figure 5b represents the uncertainty of the gravity signals obtained for the complete postseismic term of the Sumatra Andaman earthquake. It can be seen that the uncertainty is higher in the north-western part of the Northern Sumatra region. In this case, the uncertainty ranges from 0.8 to 1.2 $\mu gals$.

Similarly, the estimated values of j and the complete post seismic term ($k * ln * \left(1 + \frac{t-t_{eq2}}{\tau_2}\right)$) of the Indian Ocean earthquake are displayed as spatial plots to know the gravity changes during and after the Indian Ocean earthquake. The figure 6a represents the coseismic gravity pattern obtained for the Indian Ocean earthquake. A Quadra-polar pattern is obtained with the dilatational and compression quadrants. The red colour on the north-east and south west represent the compressional quadrant. The blue colour on the north-west and south east represent the dilatational quadrant. In this figure 6a, the centre of the quadra-polar pattern is near the epicentre of the Indian Ocean earthquake (Green dot in figure 6a).Figure 6b represents the uncertainty of the gravity signals obtained for the coseismic term of the Indian Ocean earthquake. It can be seen that the uncertainty is higher to the east of Malaysia and south of Cambodia. The uncertainty ranges from 1.061 – 1.068 $\mu gals$.

Subsequently, the figure 7a represents the complete postseismic term of the Indian Ocean earthquake ($k * ln * \left(1 + \frac{t-t_{eq2}}{\tau_2}\right)$)–(equation for the complete postseismic term). To represent this complete postseismic term of the Indian Ocean earthquake as a spatial plot as shown in the figure 7a, t value was taken 14(Last epoch considered in the time series. The time series starts with 0 representing the year 2002 and 14 representing the year 2016). In addition to this, t_{eq2} was taken as the epoch in which the Indian Ocean earthquake happened (in terms of years with the actual day represented in decimal following the number that represents the year in which the earthquake occurred in accordance to the considered time series.), estimated k and τ_2(18.441- estimated value for the relaxation time of 2012 earthquake) values were also taken and substituted in the equation shown for the complete postseismic term. Therefore, the figure 7a represents the gravity patterns obtained after the 2012 earthquake. Similarly, figure 7b has the similar uncertainty pattern as shown in figure 7a, but the uncertainty is higher in this case as it ranges from 10 – 40 $\mu gals$.

To understand the behaviour of the gravity change in a particular region or in a particular grid, time series analysis is done for that particular region or point (in my case refers a grid of size 1°*1°). With the time series analysis, one can learn the gravity changes associated to that region throughout the considered time series. It can clearly represent the jump in the gravity signals associated with the first and the second earthquake (Sumatra and Indian Ocean earthquake respectively). Finally, it can be compared to the spatial plots to draw validate and to draw further conclusion. In this report, time series are divided as 3 sets:

=> First set: Each point is chosen on each of the four quadrants obtained in the coseismic gravity pattern of the Indian Ocean earthquake.

=> Second set: Some Interior points were chosen to identify the gravity jumps

=> Third set: Points in the outer region to identify other signals.

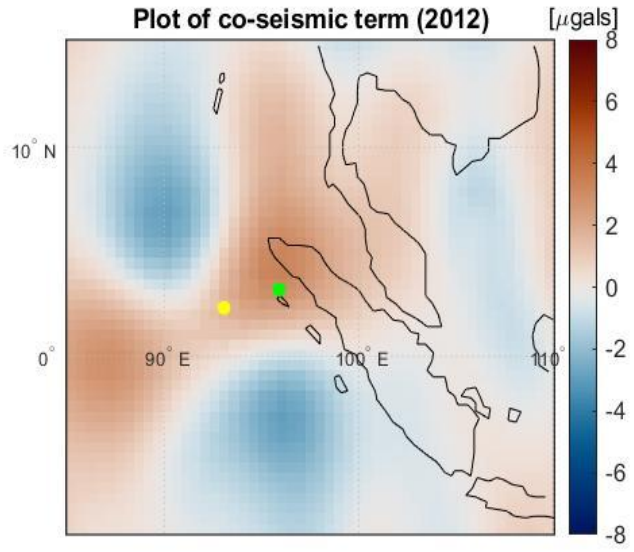

Figure 6a: Represents the coseismic gravity pattern for the Indian Ocean earthquake. (Green dot represents the epicentre of the Sumatra earthquake and yellow dot represents the epicentre of the Indian Ocean earthquake)

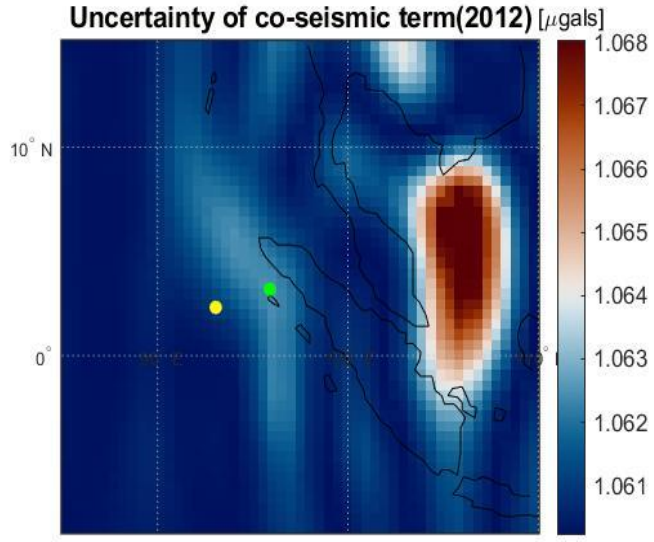

Figure 6b: Represents the uncertainty for the gravity signals of the coseismic term for the Indian Ocean earthquake. (Green dot represents the epicentre of the Sumatra earthquake and yellow dot represents the epicentre of the Indian Ocean earthquake)

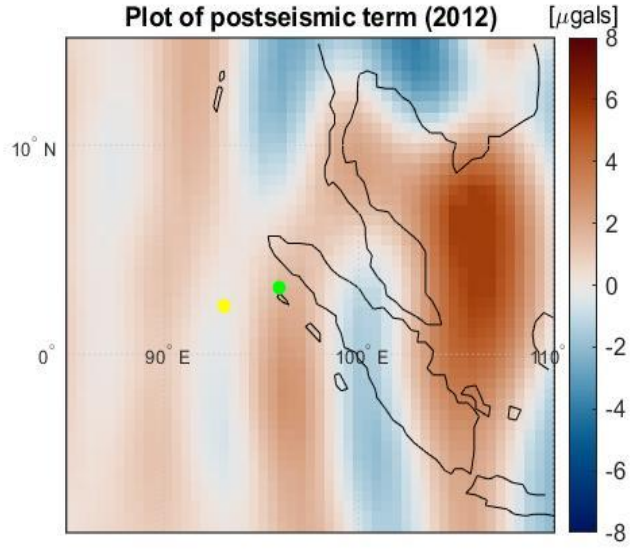

Figure 7a: Represents the postseismic gravity pattern for the Indian Ocean earthquake. (Green dot represents the epicentre of the Sumatra earthquake and yellow dot represents the epicentre of the Indian Ocean earthquake)

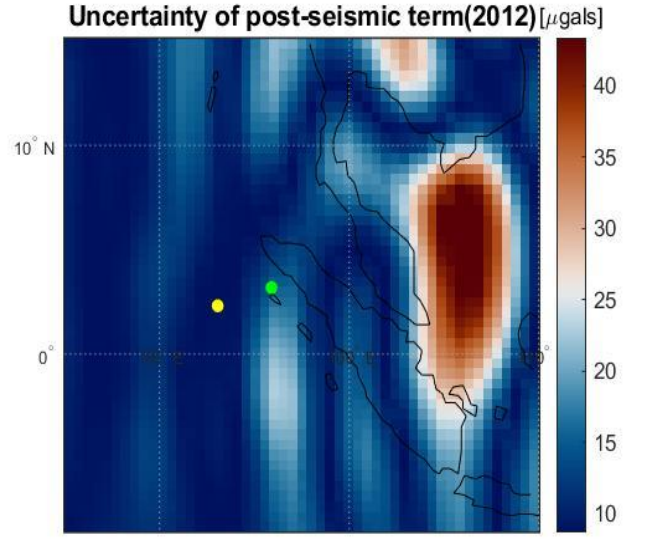

Figure 7b: Represents the uncertainty for the gravity signals of the complete postseismic term for the Indian Ocean earthquake. (Green dot represents the epicentre of the Sumatra earthquake and yellow dot represents the epicentre of the Indian Ocean earthquake)

Time series:

=> First set and their time series: 89°E and 9°N (North-west dilatational quadrant), 94°E and 5°N (North-east compressional quadrant), 87°E and 5°S (South-west compressional quadrant), 95°E and 5°S (South-east dilatational quadrant).

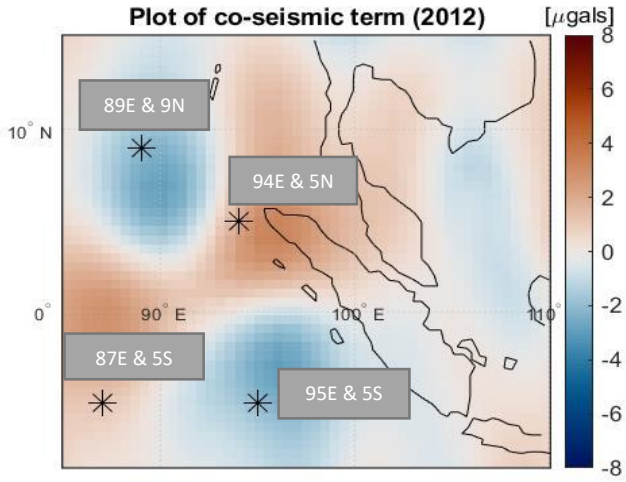

Figure 8: Represents the coseismic spatial plot of 2012 earthquake with four points. Each of the point is chosen for one quadrant in the gravity pattern and their time series are plotted in the figures below.

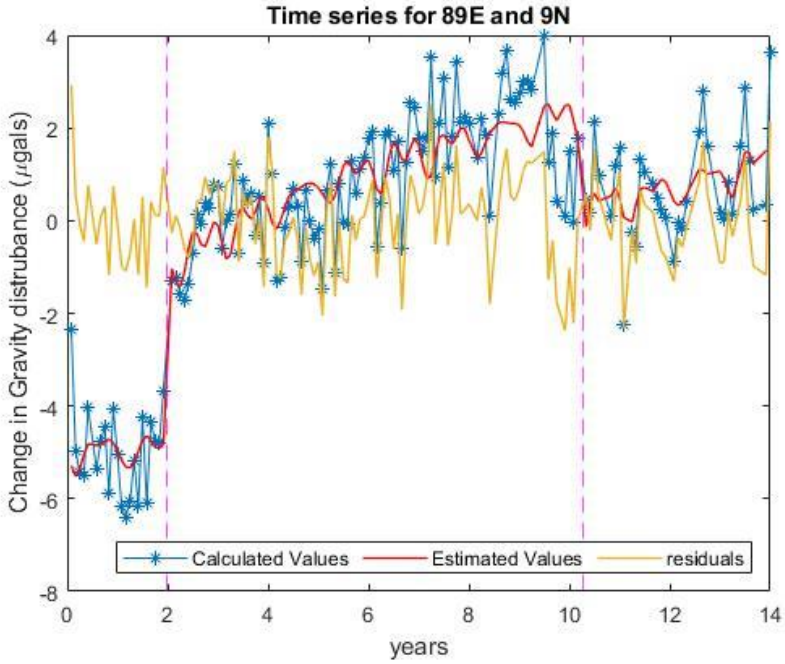

Figure 9: Time series for 89E and 9N (Point shown in figure 8). The x-axis represents the time in years (with 0 referring to the year 2002 and 14 referring to year 2016. The two magenta lines represents the epochs at which the earthquake occurred, first referring the Sumatra earthquake and second referring to the Indian Ocean earthquake.)

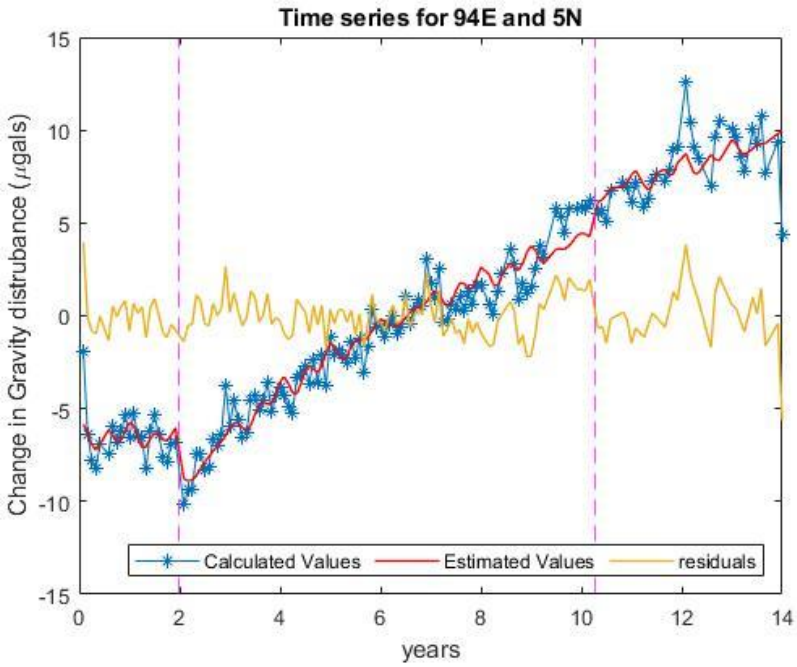

Figure 10: Time series for 94E and 5N (Point shown in figure 8). The x-axis represents the time in years (with 0 referring to the year 2002 and 14 referring to year 2016. The two magenta lines represents the epochs at which the earthquake occurred, first referring the Sumatra earthquake and second referring to the Indian Ocean earthquake.)

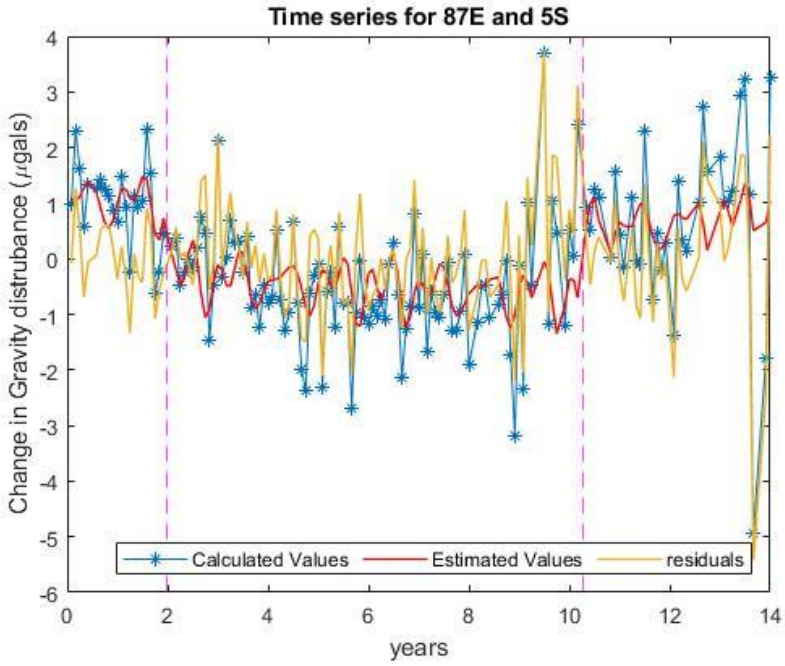

Figure 11: Time series for 87E and 5S (Point shown in figure 8). The x-axis represents the time in years (with 0 referring to the year 2002 and 14 referring to year 2016. The two magenta lines represents the epochs at which the earthquake occurred, first referring the Sumatra earthquake and second referring to the Indian Ocean earthquake.)

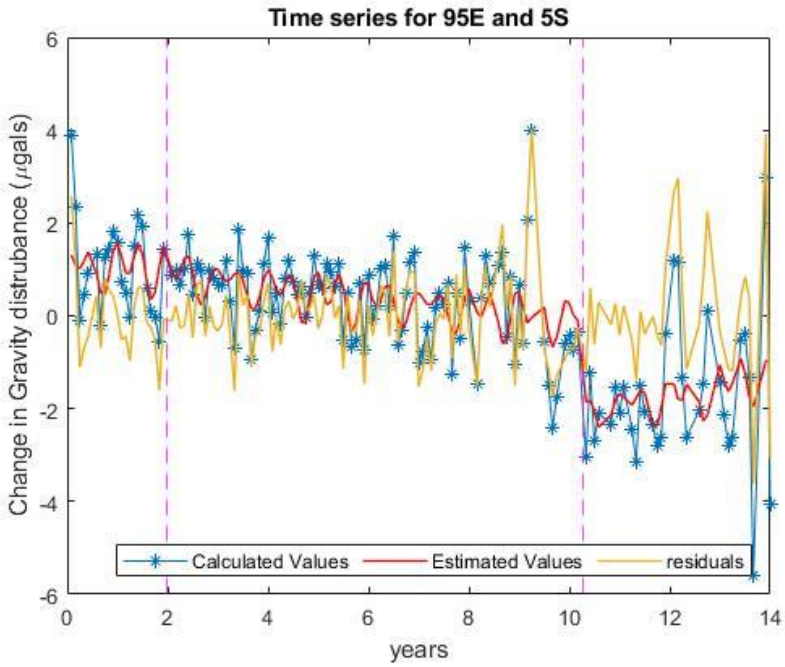

Figure 12: ***Time series for 95E and 5S (Point shown in figure 8). The x-axis represents the time in years (with 0 referring to the year 2002 and 14 referring to year 2016. The two magenta lines represents the epochs at which the earthquake occurred, first referring the Sumatra earthquake and second referring to the Indian Ocean earthquake.)***

=> Second set of points: (Interior points) 95°E and 3°N, 97°E and 5°N, 93°E and 3°N, 104°E and 2°N

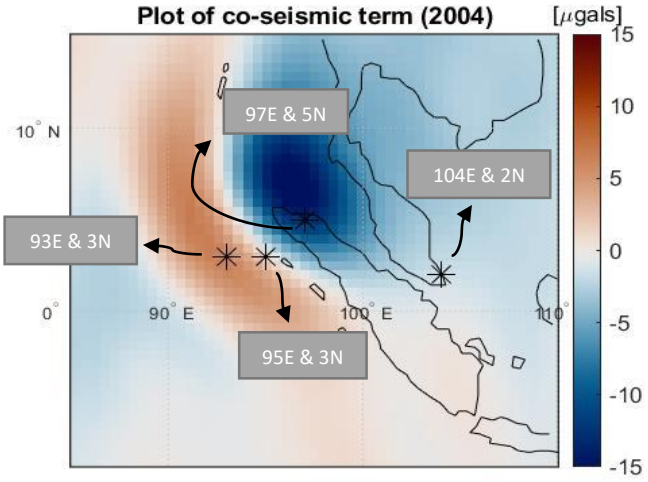

Figure 13: Represents the spatial plot with the points chosen to represent the time series. These points are chosen to identify the jumps in the gravity signal during and after the earthquakes (represented in time series).The chosen points are represented as time series in the following figures.

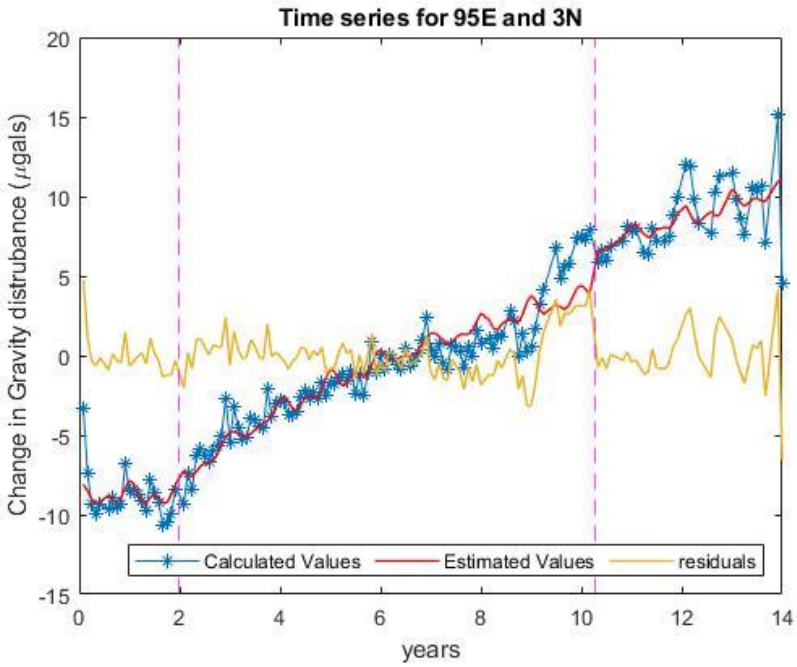

Figure 14: Time series for 95E and 3N (Point shown in figure 13). The x-axis represents the time in years (with 0 referring to the year 2002 and 14 referring to year 2016. The two magenta lines represents the epochs at which the earthquake occurred, first referring the Sumatra earthquake and second referring to the Indian Ocean earthquake.)

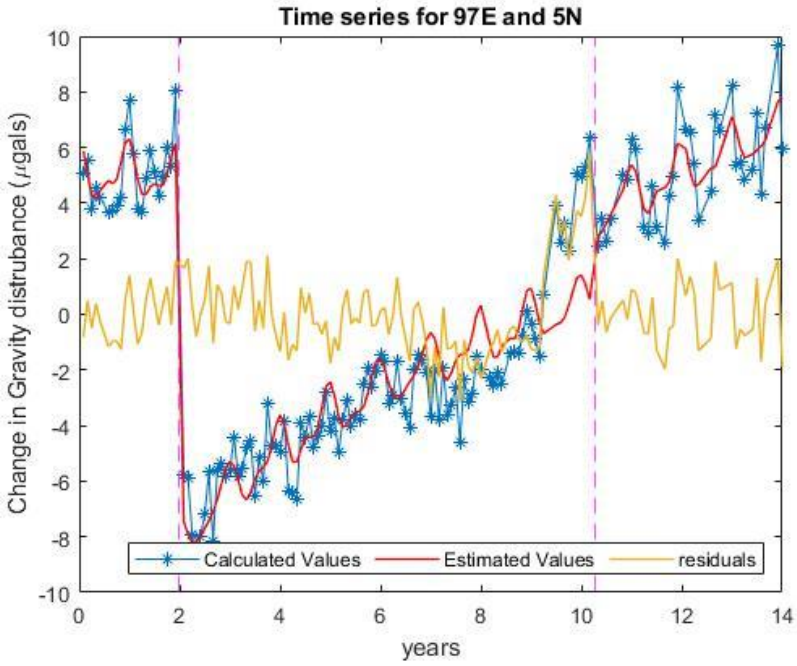

Figure 15: Time series for 97E and 5N (point shown in figure 13). The x-axis represents the time in years (with 0 referring to the year 2002 and 14 referring to year 2016. The two magenta lines represents the epochs at which the earthquake occurred, first referring the Sumatra earthquake and second referring to the Indian Ocean earthquake.)

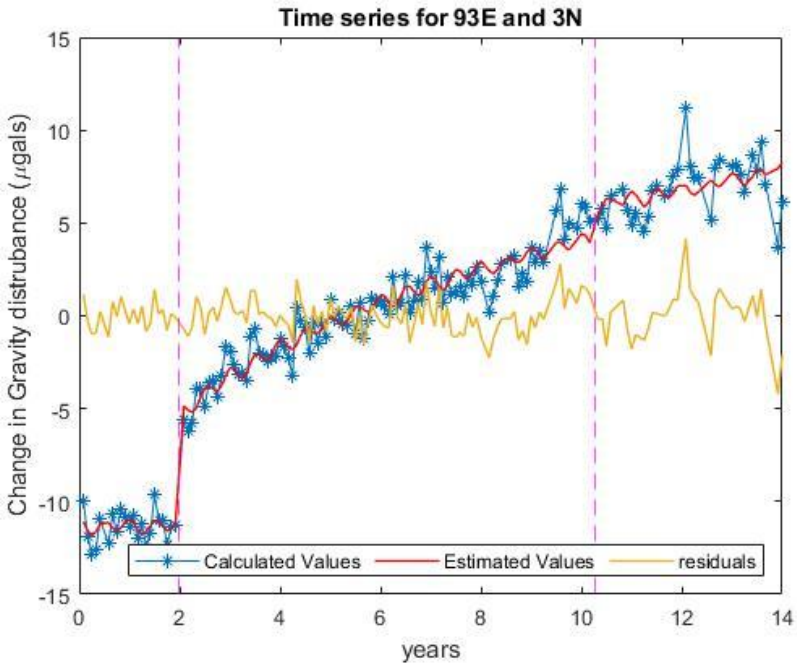

Figure 16: Time series for 93E and 3N (point shown in figure 13). The x-axis represents the time in years (with 0 referring to the year 2002 and 14 referring to year 2016. The two magenta lines represents the epochs at which the earthquake occurred, first referring the Sumatra earthquake and second referring to the Indian Ocean earthquake.)

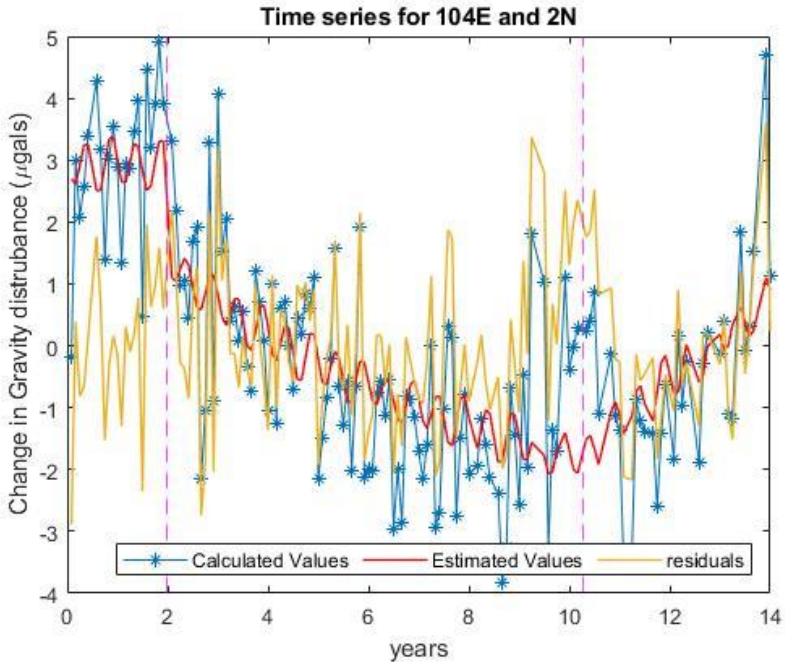

Figure 17: Time series for 104E and 2N (point shown in figure 13). The x-axis represents the time in years (with 0 referring to the year 2002 and 14 referring to year 2016. The two magenta lines represents the epochs at which the earthquake occurred, first referring the Sumatra earthquake and second referring to the Indian Ocean earthquake.)

=> Third set: (Exterior points) 87°E and 9°N, 101°E and 11°N, 105°E and 9°N , 105°E and 3°N

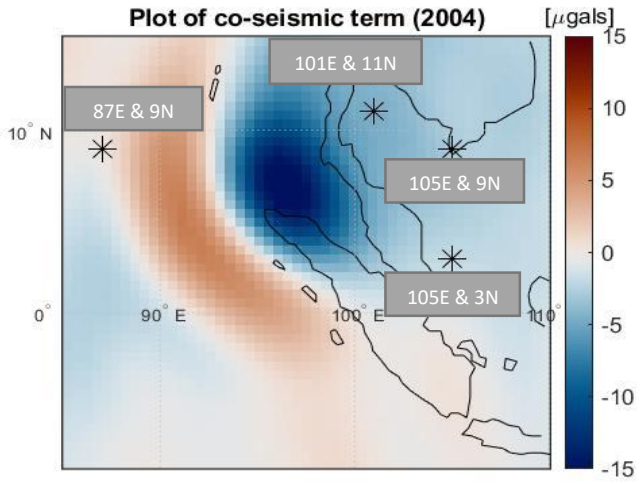

Figure 18: Represents the spatial plot with the points whose time series are plotted in the following figures.

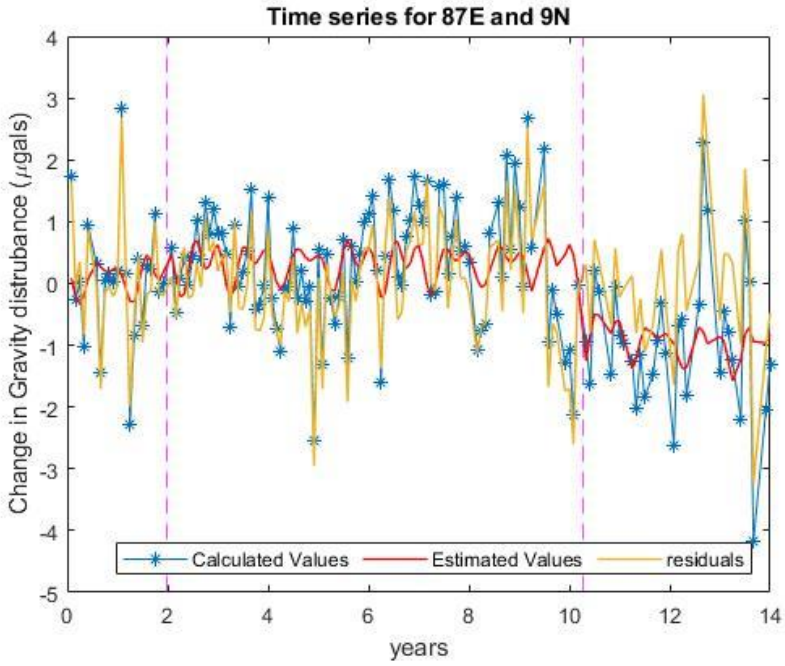

Figure 19: Time series for 87E and 9N (point shown in figure 18). The x-axis represents the time in years (with 0 referring to the year 2002 and 14 referring to year 2016. The two magenta lines represents the epochs at which the earthquake occurred, first referring the Sumatra earthquake and second referring to the Indian Ocean earthquake.)

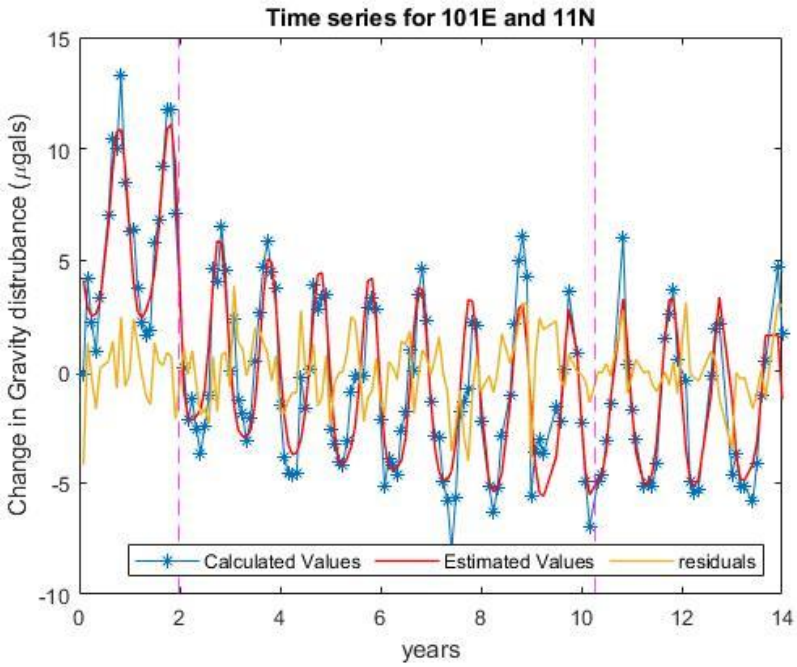

Figure 20: Time series for 101E and 11N (point shown in figure 18). The x-axis represents the time in years (with 0 referring to the year 2002 and 14 referring to year 2016. The two magenta lines represents the epochs at which the earthquake occurred, first referring the Sumatra earthquake and second referring to the Indian Ocean earthquake.)

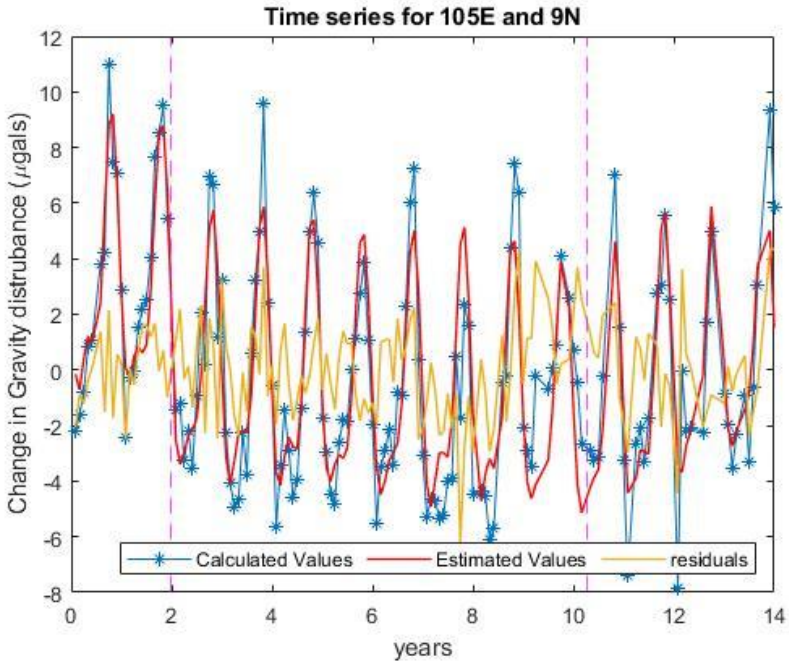

Figure 21: Time series for 105E and 9N (point shown in figure 18). The x-axis represents the time in years (with 0 referring to the year 2002 and 14 referring to year 2016. The two magenta lines represents the epochs at which the earthquake occurred, first referring the Sumatra earthquake and second referring to the Indian Ocean earthquake.)

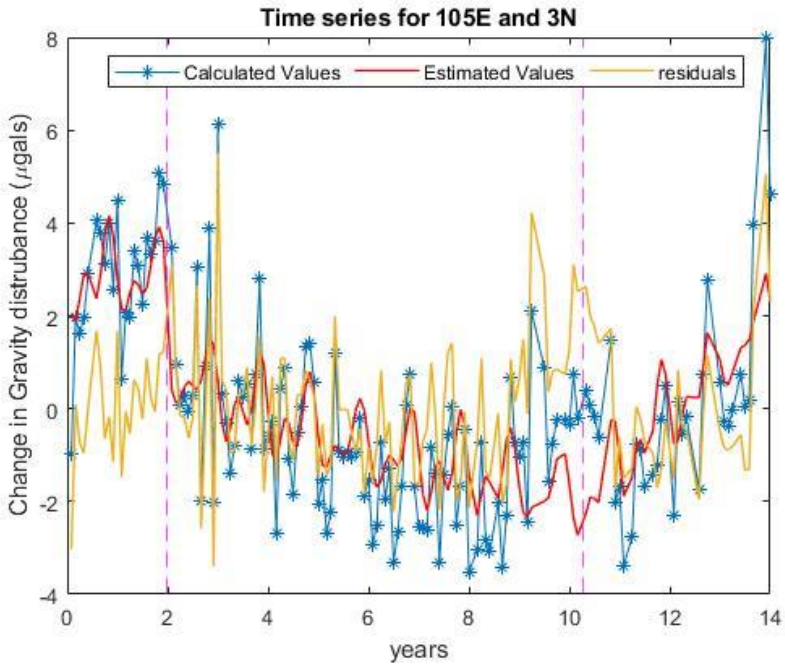

Figure 22: Time series for 105E and 3N (point shown in figure 18). The x-axis represents the time in years (with 0 referring to the year 2002 and 14 referring to year 2016. The two magenta lines represents the epochs at which the earthquake occurred, first referring the Sumatra earthquake and second referring to the Indian Ocean earthquake.)

Following the time series, figure 23 represents the root mean square (rms) of the residues of the gravity disturbances (complete time series is taken to find the root mean square). The largest rms is mostly found in the region of Cambodia, Mekong, Thailand and the Northern Sumatra region.

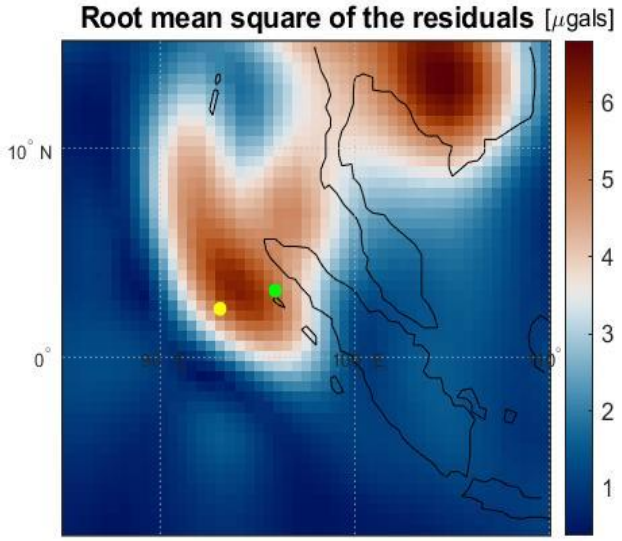

Figure 23: Represents the Root mean square of the residuals of the gravity disturbances. (In this case residual means the difference between the calculated gravity disturbances and estimated gravity disturbances)

5. Discussion and Conclusion:

As previously explained, the spatial plots obtained in the figure 4a and 5a represent the gravity patterns obtained during and after the Sumatra earthquake respectively. The coseismic gravity pattern (in figure 4a) has a strong dipole with negative gravity change present to the east of the Sunda trench and positive gravity change present to the west of the Sunda trench (banana shaped extending from 0° to 15°N) . Gravity decrease of around 15 $\mu gals$ can be seen in the spatial plot. To validate this value of gravity decrease, the gravity jump from 8 $\mu gals$ to -8 $\mu gals$ can be seen in figure 15 (Time series for 97E and 5N) during the epoch of the Sumatra earthquake. This clearly explains the coseismic gravity decrease during the 2004 earthquake. Similarly, the coseismic gravity increase is around 6-7 $\mu gals$ which can be seen in figure 16 (Time series for 93E and 3N). The gravity jump can be seen at the epoch of the 2004 earthquake in figure 16 from -12 $\mu gals$ to -5 $\mu gals$ (approximately). As the gravity disturbances are sensitive to the internal mass redistribution, the negative gravity change would have happened due to the subsidence and dilation in the Andaman Sea (east of the trench) and positive gravity change would have been due to the compression and the uplift in the west of the trench. Finally, the pattern obtained for coseismic gravity change of 2004 earthquake is quite similar to the pattern obtained in the previous studies for coseismic gravity change of 2004 earthquake (e.g., Broerse, Riva, Simons, Govers & Vermeersen, 2015; de Linage et al., 2009; Han, Shum, Bevis, Ji & Kuo 2006).

Similarly, figure 5a represents the postseismic gravity change obtained for the Sumatra earthquake. In this case, the gravity changes are different from the coseismic gravity change. Tri-polar pattern is obtained with the gravity increase at the centre (in the Northern Sumatra region) and gravity decrease on either sides. The gravity increase is around 15 $\mu gals$ and this can be seen in figure 10. In figure 10, the gravity jump can be seen from ~ (-10 $\mu gals$ to 6 $\mu gals$) (between the epochs of the Sumatra earthquake and the Indian Ocean earthquake). On other hand, there is a decrease in gravity of around 4-6 $\mu gals$ on either side. This can be seen in the figure 17 between the epochs of the two earthquakes where the gravity jumps from 2 to -2 $\mu gals$. The postseismic gravity increase could be possibly due to the viscoelastic relaxation or mantle water diffusion (Ogawa & Heki , 2007; Panet et al., 2010) . Finally, the pattern obtained for postseismic gravity changes of 2004 earthquake is similar to the pattern obtained in the previous studies for postseismic gravity changes of the same earthquake. (e.g., Broerse, Riva, Simons, Govers & Vermeersen, 2015; de Linage et al., 2009)

The uncertainty obtained for the coseismic gravity change has a similar pattern to the uncertainty obtained for postseismic gravity change. Therefore, the pattern is similar but the value range differs and the uncertainty is higher in the postseismic gravity change (from figure 4b and 5b). The pattern in the uncertainty obtained for the postseismic gravity change & coseismic gravity change coincides with some of the regions with high rms in figure 23. This uncertainty could have been caused due to the oceanic signals (de Linage et al., 2009). This can be clearly seen in the residuals plotted in figure 15 where it jumps to 6 $\mu gals$ between the epochs of the two earthquakes.

Figure 6a and 7a represents the coseismic gravity change and postseismic gravity change of the Indian Ocean earthquake respectively. The coseismic gravity change has a quadrapolar pattern with compressional and dilatational quadrants. In the compressional quadrant (North-east), positive gravity change due to compression was larger than the negative gravity change due to the subsidence (Han, Sauber & Pollitz, 2015). Positive gravity change is around 4 to 5 $\mu gals$. This gravity jump can be seen in the figure 15 from 0 to 6 $\mu gals$ (approximately) present at the epoch of the second earthquake (Indian Ocean earthquake). Similarly, positive gravity change can be observed in the south-west compressional quadrant. In this case, the gravity change is around 2-3 $\mu gals$. This can be seen in the epoch of the second earthquake in figure 11. On the other hand the north-west and south-east quadrant represent the dilatational quadrant. The negative gravity change due to the expansion is much higher than the uplift created in the sea floor. Therefore, one can observe negative gravity change in the dilatational quadrant (Han, Sauber & Pollitz, 2015). The coseismic negative gravity change is around 2-3 $\mu gals$ which can be seen in the epoch of the second earthquake in figure 9 and 12. This clearly explains the GRACE sensitive to the internal density variation and the mass redistribution. This also explains that, GRACE is more sensitive to internal mass redistribution rather than the vertical surface displacements.

Similarly, figure 7a represent the postseismic gravity change obtained for 2012 earthquake. The pattern is quite different from the pattern obtained for coseismic gravity change (2012 earthquake). In this case, postseismic uplift can be seen in the compressional quadrant. On other hand, subsidence can be seen in the dilatational quadrant (Han, Sauber & Pollitz, 2015). In addition to this, the uncertainty pattern for coseismic gravity change (2012 earthquake) is similar to the uncertainty pattern obtained for postseismic gravity change. The pattern is similar but the value range differs. The uncertainty obtained for the postseismic gravity change (2012 earthquake) is high. This uncertainty is not shown much in the rms of the complete time series (figure 23). The dominance of the Sumatra earthquake signals and the hydrological signals could have been one of the possible reasons. The postseismic estimate for 2012 earthquake can also be from ocean masses and not proper earthquake signals. Therefore, it is not a surprise that uncertainties of the postseismic gravity changes of 2012 earthquake is high.

In figure 23, there are regions of high rms near Cambodia and Thailand. This can be seen in the residual plotted for figure 20 and figure 21. Hydrological signals could have been the reason for high rms in these areas. Finally, the relaxation time was calculated as 3.169 years for the Sumatra earthquake from the non-linear inversion. This seems to be reliable as the value falls in the range (2.9 – 5 years) specified in (Broerse, Riva, Simons, Govers & Vermeersen, 2015). On other hand, the relaxation time for Indian Ocean earthquake was 18.441 years.

From the above spatial plots and the time series, it is clear that the decoupling of coseismic and postseismic gravity signals of Sumatra earthquake has been done from the coseismic and postseismic gravity signals of Indian Ocean earthquake. In addition to this, the decoupled results are compared to the previous studies, which clearly explains that the results obtained are reliable and can be made more accurate with better processing techniques. Therefore, there is a possibility of separating coseismic and postseismic earthquake signal of one earthquake from the other which is present in the same region with some temporal gap. In addition to this, it is clear that the GRACE

is more sensitive to internal mass redistribution or density changes than the vertical surface motions.

6. Reference:

[1] Tsunami Generation from the 2004 M=9.1 Sumatra-Andaman Earthquake. (2019). Retrieved 20 October 2019, from https://www.usgs.gov/centers/pcmsc/science/tsunami-generation-2004-m91-sumatra-andaman-earthquake?qt-science_center_objects=0#qt-science_center_objects

[2] Kvas, A., Behzadpour, S., Ellmer, M., Klinger, B., Strasser, S., Zehentner, N., & Mayer-Gürr, T. (2019). ITSG-Grace2018: Overview and Evaluation of a New GRACE-Only Gravity Field Time Series. *Journal of Geophysical Research: Solid Earth*.

[3] Broerse, T., Riva, R., Simons, W., Govers, R., & Vermeersen, B. (2015). Postseismic GRACE and GPS observations indicate a rheology contrast above and below the Sumatra slab. *Journal of Geophysical Research: Solid Earth*, *120*(7), 5343-5361.

[4] Han, S., Shum, C., Bevis, M., & Kuo, C. (2006). Crustal Dilatation Observed by GRACE after the 2004 Sumatra-Andaman Earthquake. *Science*, *313*(5787), 658-662. doi: 10.1126/science.1128661

[5] de Linage, C., Rivera, L., Hinderer, J., Boy, J., Rogister, Y., Lambotte, S., & Biancale, R. (2009). Separation of coseismic and postseismic gravity changes for the 2004 Sumatra-Andaman earthquake from 4.6 year of GRACE observations and modelling of the coseismic change by normal-modes summation. *Geophysical Journal International*, *176*(3), 695-714.

[6] Han, S., Riva, R., Sauber, J., & Okal, E. (2013). Source parameter inversion for recent great earthquakes from a decade-long observation of global gravity fields. *Journal of Geophysical Research: Solid Earth*, *118*(3), 1240-1267.

[7] Han, S., Sauber, J., & Pollitz, F. (2015). Coseismic compression/dilatation and viscoelastic uplift/subsidence following the 2012 Indian Ocean earthquakes quantified from satellite gravity observations. *Geophysical Research Letters*, *42*(10), 3764-3772.

[8] Broerse, D., Vermeersen, L., Riva, R., & van der Wal, W. (2011). Ocean contribution to coseismic crustal deformation and geoid anomalies: Application to the 2004 December 26 Sumatra–Andaman earthquake. *Earth and Planetary Science Letters*, *305*(3-4), 341-349.

[9] Ogawa, R., & Heki, K. (2007). Slow postseismic recovery of geoid depression formed by the 2004 Sumatra-Andaman Earthquake by mantle water diffusion. *Geophysical Research Letters*, *34*(6).

[10] Panet, I., Pollitz, F., Mikhailov, V., Diament, M., Banerjee, P., & Grijalva, K. (2010). Upper mantle rheology from GRACE and GPS postseismic deformation after the 2004 Sumatra-Andaman earthquake. *Geochemistry, Geophysics, Geosystems*, *11*(6), n/a-n/a. doi: 10.1029/2009gc002905

[11] In regards with Sumatra Andaman Earthquake (2004), https://earthquake.usgs.gov/earthquakes/eventpage/official20041226005853450_30/executive

[12] In regards with Indian Ocean Earthquake (2012), https://earthquake.usgs.gov/earthquakes/eventpage/official20050328160936530_30/executive

[13] Formulas for the calculation of gravity disturbances was taken from the notes provided by Professor Pavel Ditmar during the course of Gravity, Geodynamics and Climate change (CIE4610)

[14] Oskin, B. (2012). Why the 2012 Sumatra Earthquake Was a Weird One. Retrieved from https://www.livescience.com/21723-sumatra-2012-earthquake-weird.html